Complete next-to-leading order QCD corrections to the photon structure functions $F_2^\gamma(x,Q^2)$ and $F_L^\gamma(x,Q^2)$

E. Laenen
Fermi National Accelerator Laboratory, P.O. Box 500, MS 106, Batavia, Illinois 60510

S. Riemersma
Department of Physics, Fondren Science Building, Southern Methodist University, Dallas, Texas 75275

J. Smith
Institute for Theoretical Physics, State University of New York at Stony Brook, Stony Brook, New York 11794-3840

W. L. van Neerven
Instituut Lorentz, University of Leiden, P.O. B. 9506, 2300 RA, Leiden, The Netherlands
(Received 20 August 1993; revised manuscript received 30 November 1993)

We present the complete next-to-leading-order QCD analysis of the photon structure functions $F_2^\gamma(x,Q^2)$ and $F_L^\gamma(x,Q^2)$ for a real photon target. In particular, we study the heavy flavor content of the structure functions which is due to two different production mechanisms: namely, collisions of a virtual photon with a real photon and with a parton. We observe that the charm contributions are noticeable for $F_2^\gamma(x,Q^2)$ as well as $F_L^\gamma(x,Q^2)$ in the x region studied.

PACS number(s): 12.38.Bx, 13.60.Hb, 13.65.+i, 14.70.Bh

I. INTRODUCTION

In the past two decades there has been considerable interest in the study of photon-photon interactions in electron-positron colliders. When one photon is virtual and the other one is almost real the analogy with deep-inelastic electron-nucleon scattering motivates the introduction of the corresponding structure functions $F_k^\gamma(x,Q^2)$ $(k=2,L)$ for the photon. The deep-inelastic structure function $F_2^\gamma(x,Q^2)$ was originally measured by the PLUTO Collaboration [1] at the DESY e^+e^- collider PETRA using single-tag events in the reactions $e^-+e^+\to e^-+e^++$hadrons. In the past several years there has been a series of new measurements at PETRA, the SLAC e^+e^- storage ring PEP, and KEK TRISTAN by several groups, including CELLO [2], TPC2γ [3], TASSO [4], JADE [5], AMY [6], VENUS [7], and TOPAZ [8]. All these groups concentrated on the measurement of the light-quark contribution to $F_2^\gamma(x,Q^2)$. The heavy-quark component (mainly charm) has been hard to extract due to problems identifying charmed particle decays, so its contribution to the data was sometimes removed according to a Monte Carlo estimate. In the near future higher-luminosity runs at TRISTAN should yield some information on heavy-quark (mainly charm) production, and this is one reason that we study it here. At this moment the available data for $F_2^\gamma(x,Q^2)$ are in the region $0.03<x<0.8$ and 0.7 $(\mathrm{GeV}/c)^2<Q^2<390$ $(\mathrm{GeV}/c)^2$. Because of the experimental limitation that $xy^2\ll 1$ [for a definition of x and y, see (2.5)], there are no data available for the longitudinal structure function $F_L^\gamma(x,Q^2)$. However, there exists some hope that $F_L^\gamma(x,Q^2)$ can be measured [9] at the CERN e^+e^- collider LEP. Finally, two-photon reactions are important to understand as background processes to the normal s-channel reactions at present and future e^+e^- colliders. These machines will have a large amount of beamstrahlung [10,11]. Therefore a basic input is the parton density in a photon, which will be modified if higher-order perturbative QCD (PQCD) corrections are included.

As far as theory is concerned, the first attempt to give a theoretical description of the photon structure function in the context of perturbative QCD was given by Witten in [12]. He suggested that both the x and the Q^2 dependence of these structure functions were calculable in PQCD at asymptotically large Q^2. Thus from a theoretical point of view this process should provide a much more thorough test of PQCD than the corresponding deep-inelastic scattering off a nucleon target, where only the Q^2 evolution of the structure functions is calculable. The original optimism subsided once it was realized that there were complications with experimental confirmation of this prediction at experimental (nonasymptotic) values of Q^2 [13,14]. For recent reviews, see [15]. In particular, there is a contamination of the purely pointlike PQCD contribution by the hadronic component of the photon. This latter piece, which is most important at small virtualities, is not calculable in PQCD and must be extracted from experimental data. One of the approaches used is to describe both the hadronic and pointlike photon contribution by parton densities in the photon, analogous to the parton densities in a hadronic target. For parametrizations see [16–21]. For a different approach, see [22].

In [19] a next-to-leading-order (NLO) analysis was carried out for the photon structure function $F_2^\gamma(x,Q^2)$. This analysis also includes the lowest-order contribution coming from heavy-flavor production, which is described by the Bethe-Heitler cross section corresponding to the

process $\gamma^*+\gamma\to Q+\bar{Q}$. In this case the mass m of the heavy flavor is not neglected with respect to Q^2, especially in the threshold region. If $Q^2\gg m^2$, one encounters large logarithmic terms containing $\ln(Q^2/m^2)$, which have to be summed using the Altarelli-Parisi (AP) equations. This procedure provides us with the heavy-flavor densities in the photon which are akin to the parton densities originating from the light quarks in the photon. The same procedure has been applied for the longitudinal structure function $F_L^\gamma(x,Q^2)$ in [23], but only in leading order.

In this paper we want to extend the above analysis by including higher-order PQCD corrections which were not considered in the literature so far. Since the NLO QCD corrections to the longitudinal coefficient functions due to massless partons [24] and heavy flavors [25] have been recently calculated, we are now also able to present an NLO analysis for $F_L^\gamma(x,Q^2)$. In addition, we can also improve our knowledge of the heavy-flavor content of $F_2^\gamma(x,Q^2)$ by including the order α_s corrections to the Bethe-Heitler process $\gamma^*+\gamma\to Q+\bar{Q}$. We also include corrections to $F_k^\gamma(x,Q^2)$ $(k=2,L)$ due to heavy-flavor production mechanisms given by the processes $\gamma^*+g\to Q+\bar{Q}$ (corrected up to order α_s^2) and

$$\gamma^*+q(\bar{q})\to Q+\bar{Q}+q(\bar{q}) ,$$

where the incoming gluon and (anti)quark originate from the on-mass-shell photon. Furthermore, we use the most recent gluon and (anti)quark densities in our analysis.

Finally, we should mention that there was a previous investigation of PQCD corrections to heavy-quark production in [26], where it was assumed that both photons were off mass shell, and a small value for the photon virtuality was chosen for generating numerical results. Since these authors did not therefore encounter mass singularities, they had no need to perform any mass factorization. Hence their method was different from the one we adopt.

The paper is organized as follows. In Sec. II we present the photonic and hadronic coefficient functions corrected up to next-to-leading order in α_s, which are needed for the photon structure functions $F_k^\gamma(x,Q^2)$ $(k=2,L)$. In Sec. III we show the differences between the leading-order (LO) and the next-to-leading-order (NLO) photon structure functions. In particular, we discuss the effect of the heavy-flavor component (mainly charm) originating from the hadronic as well as the pointlike photon interactions.

II. HIGHER-ORDER CORRECTIONS TO THE PHOTON STRUCTURE FUNCTIONS

The deep-inelastic photon structure functions denoted by $F_k^\gamma(x,Q^2)$ $(k=2,L)$ are measured in e^-e^+ collisions via the process (see Fig. 1)

$$e^-(p_e)+e^+\to e^-(p_e')+e^++X , \tag{2.1}$$

where X denotes any hadronic state which is allowed by quantum-number conservation laws. When the outgoing electron is tagged, then the above reaction is dominated

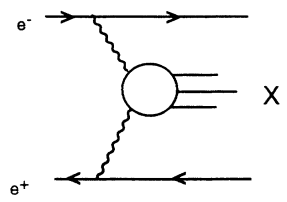

FIG. 1. The process $e^-(p_e)+e^+\to e^-(p_e')+e^++X$, where X denotes any hadronic state.

by the photon-photon collision reaction (see Fig. 1)

$$\gamma^*(q)+\gamma(k)\to X , \tag{2.2}$$

where one of the photons is highly virtual and the other one is almost on mass shell. The process (2.1) is described by the cross section

$$\frac{d^2\sigma}{dxdy}=\int dzzf_\gamma^e\left[z,\frac{S}{m_e^2}\right]\frac{2\pi\alpha^2S}{Q^4}\times\{[1+(1-y)^2]F_2^\gamma(x,Q^2)-y^2F_L^\gamma(x,Q^2)\} , \tag{2.3}$$

where $F_k^\gamma(x,Q^2)$ $(k=2,L)$ denote the deep-inelastic photon structure functions and $\alpha=e^2/4\pi$ is the fine-structure constant. Furthermore, the off-mass-shell photon and the on-mass-shell photon are indicated by the four-momenta q and k, respectively, with $q^2=-Q^2<0$ and $k^2\approx 0$. Because the photon with momentum k is almost on mass shell, expression (2.3) is written in the Weizsäcker-Williams approximation. In this approximation the function $f_\gamma^e(z,S/m_e^2)$ is the probability of finding a photon $\gamma(k)$ in the positron (see Fig. 1). The fraction of the energy of the positron carried off by the photon is denoted by z while $\sqrt{S}$ is the c.m. energy of the electron-positron system. The function $f_\gamma^e(z,S/m_e^2)$ is given by (see [27])

$$f_\gamma^e\left[z,\frac{S}{m_e^2}\right]=\frac{\alpha}{2\pi}\frac{1+(1-z)^2}{z}\ln\frac{(1-z)(zS-4m^2)}{z^2m_e^2} , \tag{2.4}$$

provided a heavy quark with mass m is produced (for light quarks, $m=0$). The scaling variables x and y are defined by

$$x=\frac{Q^2}{2k\cdot q},\quad y=\frac{k\cdot q}{k\cdot p_e},\quad q=p_e-p_e' , \tag{2.5}$$

where p_e,p_e' are the momenta of the incoming and outgoing electron, respectively. Following the procedure in [28] the photon structure functions in the QCD-improved parton model have the form

$$\frac{1}{\alpha}F_k^\gamma(x,Q^2)=x\int_x^1\frac{dz}{z}\left\{\left[\frac{1}{n_f}\sum_{i=1}^{n_f}e_i^2\right]\left[\Sigma^\gamma\left[\frac{x}{z},M^2\right]\mathcal{C}_{k,q}^{\mathrm{S}}\left[z,\frac{Q^2}{M^2}\right]+g^\gamma\left[\frac{x}{z},M^2\right]\mathcal{C}_{k,g}\left[z,\frac{Q^2}{M^2}\right]\right]\right.$$
$$\left.+\Delta^\gamma\left[\frac{x}{z},M^2\right]\mathcal{C}_{k,q}^{\mathrm{NS}}\left[z,\frac{Q^2}{M^2}\right]\right\}$$
$$+x\int_x^{z_{\max}}\frac{dz}{z}\left\{\left[\frac{1}{n_f}\sum_{i=1}^{n_f}e_i^2\right]\left[\Sigma^\gamma\left[\frac{x}{z},M^2\right]\mathcal{C}_{k,q}^{\mathrm{S}}\left[z,\frac{Q^2}{M^2},m^2\right]+g^\gamma\left[\frac{x}{z},M^2\right]\mathcal{C}_{k,g}\left[z,\frac{Q^2}{M^2},m^2\right]\right]\right.$$
$$\left.+\Delta^\gamma\left[\frac{x}{z},M^2\right]\mathcal{C}_{k,q}^{\mathrm{NS}}\left[z,\frac{Q^2}{M^2},m^2\right]\right\}$$
$$+x\int_x^{z_{\max}}\frac{dz}{z}\left\{e_H^2\left[\Sigma^\gamma\left[\frac{x}{z},M^2\right]\mathcal{C}_{k,q}^{H}\left[z,\frac{Q^2}{M^2},m^2\right]+g^\gamma\left[\frac{x}{z},M^2\right]\mathcal{C}_{k,g}^{H}\left[z,\frac{Q^2}{M^2},m^2\right]\right]\right\}$$
$$+\frac{3}{4\pi}x\left[\left[\sum_{i=1}^{n_f}e_i^4\right]\mathcal{C}_{k,\gamma}\left[x,\frac{Q^2}{M^2}\right]+e_H^4\mathcal{C}_{k,\gamma}^{H}\left[x,Q^2,m^2\right]\right], \tag{2.6}$$

where the meaning of the symbols is explained below.

The quantities Σ^γ and Δ^γ represent the singlet and nonsinglet combinations of the quark densities in the photon, respectively, while the gluon density is represented by g^γ. The same flavor decomposition is also applied to the hadronic (Wilson) coefficient functions $\mathcal{C}_{k,i}(i=q,g)$ so that $\mathcal{C}_{k,g}^{\mathrm{S}}(z,Q^2/M^2)$ and $\mathcal{C}_{k,q}^{\mathrm{NS}}(z,Q^2/M^2)$ stand for the singlet and nonsinglet coefficient functions, respectively, and $\mathcal{C}_{k,g}(z,Q^2/M^2)$ denotes the gluonic coefficient function, where M^2 is the mass factorization scale. The hadronic coefficient functions can be attributed to hard processes with a light quark or gluon in the initial state, such as $\gamma^*+q\to q+g$ or $\gamma^*+g\to q+\bar{q}$, where the initial parton emerges from the real (on-mass-shell) photon. Hence they are multiplied by the corresponding parton densities in the photon.

We also make a distinction between light- and heavy-flavor contributions to the coefficient functions. The latter are indicated by their explicit dependence on the heavy-flavor mass m. For example, in the contribution to $\mathcal{C}_{k,i}(z,Q^2/M^2,m^2)$ [second part of (2.6)] the virtual photon is attached either to the incoming light quark, as is the case in the reaction $\gamma^*+q\to q+Q+\bar{Q}$, or indirectly to the incoming gluon. Actually, the $\mathcal{C}_{k,i}(z,Q^2/M^2,m^2)$ belong to the same class as the hadronic light-parton coefficient functions presented in the first part of expression (2.6). The only difference is that $\mathcal{C}_{k,i}(z,Q^2/M^2,m^2)$ receives contributions from a heavy-flavor pair produced in the final state.

In the third set of terms in (2.6) the heavy-flavor coefficient functions originate from subprocesses where the virtual photon is attached to one of the outgoing heavy flavors, as, for example, in $\gamma^*+g\to Q+\bar{Q}$; so they are given an additional superscript H. Finally, the fourth set of terms in (2.6) contains the photonic coefficient functions indicated by $\mathcal{C}_{k,\gamma}$ coming from reactions such as $\gamma^*+\gamma\to q+\bar{q}$ or $\gamma^*+\gamma\to Q+\bar{Q}$. These originate from hard processes where the (on-shell) real photon is directly attached to the light or heavy quarks produced in the final state so there is no need for any convolution integral.

The index i in (2.6) runs over all light active flavors whose number is given by n_f and e_i,e_H stand for the charges of the light and heavy quarks, respectively, in units of e. The upper boundary of the integrals in (2.6) containing the convolution of the parton densities with the heavy-flavor coefficient functions is given by

$$z_{\max}=\frac{Q^2}{4m^2+Q^2}\ . \tag{2.7}$$

The parton densities as well as the coefficient functions depend on the mass factorization scale M except for the $\mathcal{C}_{k,\gamma}^{H}$, which can be calculated in PQCD without performing mass factorization. Notice that in addition to the mass factorization scale M the quantities in (2.6) also depend on the renormalization scale R which appears in the PQCD corrections via $\alpha_s(R^2)$. However, in this paper we will put $R=M$.

According to the origin of the photonic parton densities and the two different types of coefficient functions, i.e., $\mathcal{C}_{k,q},\mathcal{C}_{k,g}$ (hadronic), and $\mathcal{C}_{k,\gamma}$ (photonic), we will call the first three terms in (2.6) (represented by the integrals) the *hadronic* photon parts, and the last term the *pointlike* photon part. Notice that both these terms are separately factorization scheme dependent as indicated by the presence of the scale M. In particular, the scheme dependence of the pointlike photon part in (2.6) is due the light-quark contribution $\mathcal{C}_{k,\gamma}(x,Q^2/M^2)$. The scheme dependence is canceled by the hadronic photon part due to the light-quark contribution, provided that the quark densities and the hadronic coefficient functions are computed in the same scheme as $\mathcal{C}_{k,\gamma}(x,Q^2/M^2)$. The hadronic heavy-flavor part is scheme independent by itself. The photonic heavy-flavor piece is obtained without having to perform mass factorization and needs no parton distribution functions, and is thus not dependent on the factorization scheme.

In the subsequent part of this section we will discuss

the contributions to the coefficient functions in (2.6) which are needed for a next-to-leading-order (NLO) description of the photon structure functions $F_2^\gamma(x,Q^2)$ and $F_L^\gamma(x,Q^2)$. The results of our calculations will be presented in the plots of Sec. III. For these NLO calculations we also have to use the next-to-leading logarithmic (NLL) approximation to the parton densities, which are given, for example, in [19–21].

Starting with the NLL parton densities, the singlet and nonsinglet combinations are written in the following way. Below the charm-quark threshold we have

$$n_f=3, \quad \sum_{i=1}^{3} e_i^2=\frac{2}{3}, \quad \sum_{i=1}^{3} e_i^4=\frac{2}{9}, \tag{2.8}$$

$$\Sigma^\gamma=u^\gamma+\bar{u}^\gamma+d^\gamma+\bar{d}^\gamma+s^\gamma+\bar{s}^\gamma, \tag{2.9}$$

$$\Delta^\gamma=\frac{1}{9}(2u^\gamma+2\bar{u}^\gamma-d^\gamma-\bar{d}^\gamma-s^\gamma-\bar{s}^\gamma). \tag{2.10}$$

Above the charm-quark threshold and below the bottom-quark threshold the above quantities are changed into

$$n_f=4, \quad \sum_{i=1}^{4} e_i^2=\frac{10}{9}, \quad \sum_{i=1}^{4} e_i^4=\frac{34}{81}, \tag{2.11}$$

$$\Sigma^\gamma=u^\gamma+\bar{u}^\gamma+d^\gamma+\bar{d}^\gamma+s^\gamma+\bar{s}^\gamma+c^\gamma+\bar{c}^\gamma, \tag{2.12}$$

$$\Delta^\gamma=\frac{1}{6}(u^\gamma+\bar{u}^\gamma+c^\gamma+\bar{c}^\gamma-d^\gamma-\bar{d}^\gamma-s^\gamma-\bar{s}^\gamma). \tag{2.13}$$

Finally, above the bottom-quark threshold they become

$$n_f=5, \quad \sum_{i=1}^{5} e_i^2=\frac{11}{9}, \quad \sum_{i=1}^{5} e_i^4=\frac{35}{81}, \tag{2.14}$$

$$\Sigma^\gamma=u^\gamma+\bar{u}^\gamma+d^\gamma+\bar{d}^\gamma+s^\gamma+\bar{s}^\gamma+c^\gamma+\bar{c}^\gamma+b^\gamma+\bar{b}^\gamma, \tag{2.15}$$

$$\Delta^\gamma=\frac{1}{15}(3u^\gamma+3\bar{u}^\gamma+3c^\gamma+3\bar{c}^\gamma-2d^\gamma-2\bar{d}^\gamma-2s^\gamma-2\bar{s}^\gamma-2b^\gamma-2\bar{b}^\gamma). \tag{2.16}$$

Because the photon is a charge-conjugate eigenstate, one can set the quark densities equal to the antiquark densities.

We will now discuss the origin of the coefficient functions $\mathcal{C}_{k,i}$ $(k=2,L)$ and $(i=q,g,\gamma)$ which appear in (2.6). Starting with the last terms, the photonic coefficient functions $\mathcal{C}_{k,\gamma}$ are given up to next-to-leading order by the following parton subprocesses. In the Born approximation the light quarks are produced by the reaction (Fig. 2)

$$\gamma^*(q)+\gamma(k)\rightarrow q+\bar{q}, \tag{2.17}$$

FIG. 2. The lowest-order Feynman diagrams contributing to the Born reaction $\gamma^*(q)+\gamma(k)\rightarrow q+\bar{q}$.

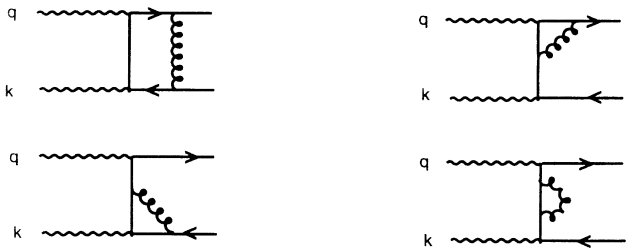

FIG. 3. Feynman diagrams contributing to the one-loop correction to the process $\gamma^*(q)+\gamma(k)\rightarrow q+\bar{q}$. Additional graphs are obtained by reversing the arrows on the quark lines. Graphs containing the external quark self-energies are included in the calculation, but are not shown in the figure.

while the heavy quarks are produced by the same reaction

$$\gamma^*(q)+\gamma(k)\rightarrow Q+\bar{Q}, \tag{2.18}$$

provided the square of the c.m. energy denoted by s, where $s=(k+q)^2$ satisfies the threshold condition $s\geq 4m^2$. The $O(\alpha_s)$ PQCD corrections are given by the one-loop contributions to processes (2.17) and (2.18) (see Fig. 3) and the gluon bremsstrahlung processes (see Fig. 4)

$$\gamma^*(q)+\gamma(k)\rightarrow q+\bar{q}+g, \tag{2.19}$$

$$\gamma^*(q)+\gamma(k)\rightarrow Q+\bar{Q}+g. \tag{2.20}$$

The parton cross section for the Born reaction in the case of light quarks (2.17) can be found in [14,29]. In the case of heavy-flavor production (2.18) the Born cross section is presented in [16,28]. Notice that the above reactions are very similar to the ones where the on-mass-shell photon $\gamma(k)$ is replaced by a gluon $g(k)$. The cross sections of the photon-induced processes constitute the Abelian parts of the expressions obtained for the gluon-induced processes, which are presented up to order α_s^2 for the case of massless quarks in [24] and in the case of massive quarks in [25]. By equating some color factors equal to unity or zero in the latter expressions, one automatically obtains the cross sections for the photon-induced process-

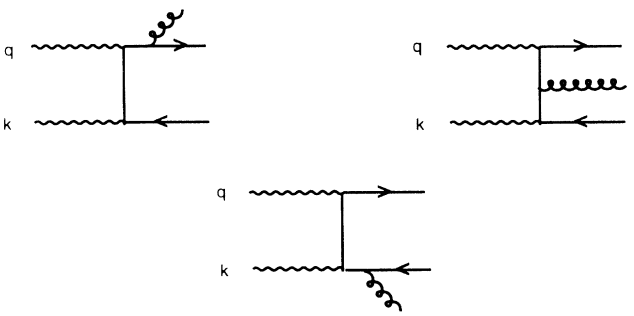

FIG. 4. The order g $(\alpha_s=g^2/4\pi)$ Feynman diagrams contributing to the gluon bremsstrahlung process $\gamma^*(q)+\gamma(k)\rightarrow q+\bar{q}+g$. Additional graphs are obtained by reversing the arrows on the quark lines.

es above, in particular, for (2.19) and (2.20) (see Appendix). In the case of massless quarks the parton cross sections for (2.17) and (2.19) contain collinear divergences which can be attributed to the initial photon being on mass shell. These singularities are removed by mass factorization in the following way. We define

$$\hat{\mathcal{F}}_{k,\gamma}(z,Q^2,\epsilon)=\sum_i \int_0^1 dz_1 \int_0^1 dz_2 \delta(z-z_1 z_2)\Gamma_{i\gamma}(z_1,M^2,\epsilon) \times \mathcal{C}_{k,i}\left[z_2,\frac{Q^2}{M^2}\right], \tag{2.21}$$

where $\hat{\mathcal{F}}_{k,\gamma}(z,Q^2,\epsilon)$ is the parton structure function, which is related to the parton cross section in the same way as the photon structure function $F_k^\gamma(x,Q^2)$ is related to the cross section $d^2\sigma/dx\,dy$ in (2.3). The parton structure function contains the collinear divergences represented by the pole terms ϵ^{-j} (j is a positive integer), where $\epsilon=n-4$ (we use dimensional regularization). These divergences are absorbed in the transition functions $\Gamma_{i\gamma}$ ($i=\gamma,q,g$), which depend both on ϵ and on the mass factorization scale M. They can be inferred from the Abelian parts of Γ_{ig} in [14,18,29,30].

Both the photonic and hadronic coefficient functions $\mathcal{C}_{k,i}$ ($i=\gamma,q,g$) which appear in the expressions for $F_2^\gamma(x,Q^2)$ and $F_L^\gamma(x,Q^2)$ in (2.6) are computed in the modified minimal subtraction ($\overline{\text{MS}}$) scheme. The coefficient functions $\mathcal{C}_{i,k}$ in (2.6) and (2.21) can be expanded in a power series in α_s as

$$\mathcal{C}_{k,i}=\mathcal{C}_{k,i}^{(0)}+\frac{\alpha_s(M^2)}{4\pi}\mathcal{C}_{k,i}^{(1)}+\left[\frac{\alpha_s(M^2)}{4\pi}\right]^2\mathcal{C}_{k,i}^{(2)}+\cdots, \tag{2.22}$$

which holds for the light- as well as the heavy-flavor contributions. The photonic coefficient functions for light quarks $\mathcal{C}_{k,\gamma}^{(0)}$ and $\mathcal{C}_{k,\gamma}^{(1)}$ can be directly derived via the mass factorization formula (2.21) from reactions (2.17) and (2.19), respectively. The heavy-flavor coefficients $\mathcal{C}_{k,\gamma}^{H,(0)}$ and $\mathcal{C}_{k,\gamma}^{H,(1)}$, which are obtained without using mass factorization, originate from processes (2.18) and (2.20). Notice that in the case of massive quarks the parton structure functions corresponding to the reactions (2.18) and (2.20) do not have collinear singularities and they can automatically be identified with the coefficient functions $\mathcal{C}_{k,\gamma}^{H}$.

Using the mass factorization formula in (2.21) one can also obtain the order α_s contributions to the hadronic coefficient functions $\mathcal{C}_{k,q}^{(1)}$ coming from process (2.19). The higher-order contributions to the hadronic coefficient functions emerge when one calculates the NLO corrections to process (2.17). For example, the gluonic coefficients $\mathcal{C}_{k,g}^{(1)}$ can be inferred from the contributions to

$$\gamma^*(q)+\gamma(k)\rightarrow q+\bar{q}+q+\bar{q}\ , \tag{2.23}$$

while $\mathcal{C}_{k,g}^{H,(1)}$ can be inferred from the contributions to

$$\gamma^*(q)+\gamma(k)\rightarrow q+\bar{q}+Q+\bar{Q}\ . \tag{2.24}$$

Fortunately there is a quicker method to obtain the same information. The hadronic coefficient functions needed for the $O(\alpha_s)$ renormalization-group improved photon structure functions $F_k^\gamma(x,Q^2)$ (2.6) can also be obtained from deep-inelastic lepton-hadron scattering, where the higher-order corrections are known. For light-flavor production we have listed the parton subprocesses and the corresponding coefficients which follow from these reactions in Table I. We have given the corresponding information for heavy-flavor production in Table II. In lowest order the photonic and hadronic coefficient functions have been presented in the literature (see [14,29,23,28]). Since these authors used a notation which is different from ours, we will present the relevant formulas below. In next-to-leading order the expressions for the coefficient functions are obtained from [24] (light quarks and gluons) and [25] (heavy quarks). However, the expressions are too long to be presented in a paper.[1] The method whereby the higher-order coefficients can be derived from the expressions in [24,25] is explained in the Appendix.

Starting with the photonic coefficients for light quarks [see reaction (2.17)] they are given by

$$C_{2,\gamma}^{(0)}\left[z,\frac{Q^2}{M^2}\right]=4[z^2+(1-z)^2]\left[\ln\frac{Q^2}{M^2}+\ln(1-z)-\ln(z)\right]+32z(1-z)-4 \tag{2.25}$$

and

$$\mathcal{C}_{L,\gamma}^{(0)}\left[z,\frac{Q^2}{M^2}\right]=16z(1-z)\ . \tag{2.26}$$

For massive quarks in the final state [see (2.18)] we have

$$\mathcal{C}_{2,\gamma}^{H,(0)}(z,Q^2,m^2)=\left\{\left[4-8z(1-z)+\frac{16m^2}{Q^2}z(1-3z)-\frac{32m^4}{Q^4}z^2\right]L+\left[-4+32z(1-z)-16\frac{m^2}{Q^2}z(1-z)\right]\left[1-\frac{4m^2}{s}\right]^{1/2}\right\} \tag{2.27}$$

[1]These functions are available from smith@elsebeth.physics.sunysb.edu

TABLE I. List of deep-inelastic virtual-photon-parton subprocesses up to $O(\alpha_s^2)$. The one- and two-loop corrections to the lower-order processes have been included in our calculations, but are not explicitly mentioned in the table.

Order	Parton subprocess	Coefficient function
α_s^0	$\gamma^*+q(\bar{q})\to q(\bar{q})$	$\mathcal{C}_{k,q}^{(0)}$
α_s^1	$\gamma^*+q(\bar{q})\to q(\bar{q})+g$	$\mathcal{C}_{k,q}^{\mathrm{NS},(1)}=\mathcal{C}_{k,q}^{\mathrm{S},(1)}$
	$\gamma^*+g\to q+\bar{q}$	$\mathcal{C}_{k,g}^{(1)}$
α_s^2	$\gamma^*+q(\bar{q})\to q(\bar{q})+g+g$	$\mathcal{C}_{k,q}^{\mathrm{NS},(2)}=\mathcal{C}_{k,q}^{\mathrm{S},(2)}$
	$\gamma^*+q(\bar{q})\to q(\bar{q})+q(\bar{q})+\bar{q}(q)$	$\mathcal{C}_{k,q}^{\mathrm{NS},(2)}\neq\mathcal{C}_{k,q}^{\mathrm{S},(2)}$
	$\gamma^*+g\to q+\bar{q}+g$	$\mathcal{C}_{k,g}^{(2)}$

and

$$\mathcal{C}_{L,\gamma}^{H,(0)}(z,Q^2,m^2)=16z(1-z)\left[\left[1-\frac{4m^2}{s}\right]^{1/2}-2\frac{m^2}{s}L\right], \tag{2.28}$$

where m is the heavy-flavor mass and $\sqrt{s}$ is the c.m. energy of the virtual photon-real photon system. Furthermore, we have

$$s=(1-z)\frac{Q^2}{z},\quad L=\ln\left[\frac{1+\sqrt{1-4m^2/s}}{1-\sqrt{1-4m^2/s}}\right]. \tag{2.29}$$

Formulas (2.27) and (2.28) can be found in [31,32].

In the next order in α_s, process (2.19) (Fig. 4) and the one-loop corrections to process (2.17) (Fig. 3) give rise to the coefficients $C_{k,\gamma}^{(1)}(z,Q^2/M^2)$. In the case that the outgoing fermion lines in Figs. 3 and 4 stand for the heavy flavors [see reactions (2.18) and (2.20)], the corresponding coefficients are given by $\mathcal{C}_{k,\gamma}^{H,(1)}(z,Q^2,m^2)$. More information about the higher-order corrections to the photonic coefficient functions can be found in the Appendix.

In zeroth order of α_s the hadronic coefficient functions are

$$\mathcal{C}_{2,q}^{(0)}\left[z,\frac{Q^2}{M^2}\right]=\delta(1-z), \tag{2.30}$$

$$\mathcal{C}_{L,q}^{(0)}\left[z,\frac{Q^2}{M^2}\right]=0, \tag{2.31}$$

$$\mathcal{C}_{k,g}^{(0)}\left[z,\frac{Q^2}{M^2}\right]=0\quad(k=2,L). \tag{2.32}$$

In order α_s the hadronic coefficient functions originating from a light quark in the initial state (Table I) are given by

$$\mathcal{C}_{2,q}^{(1)}\left[z,\frac{Q^2}{M^2}\right]=C_F\left\{\left[\left[\frac{4}{1-z}\right]_+-2-2z\right]\left[\ln\frac{Q^2}{M^2}+\ln(1-z)-\frac{3}{4}\right]\right.$$

$$\left.-2\frac{1+z^2}{1-z}\ln z+\frac{9}{2}+\frac{5}{2}z+\delta(1-z)\left[3\ln\frac{Q^2}{M^2}-9-4\zeta(2)\right]\right\}, \tag{2.33}$$

where the standard definition of a plus distribution is used, and

$$\mathcal{C}_{L,q}^{(1)}\left[z,\frac{Q^2}{M^2}\right]=C_F[4z]. \tag{2.34}$$

Notice that in order α_s there is no difference between $\mathcal{C}_{k,q}^{\mathrm{S},(1)}$ and $\mathcal{C}_{k,q}^{\mathrm{NS},(1)}$. The coefficient functions for a gluon in the initial state and massless quarks in the final state (Table I) can be derived from (2.25) and (2.26) via multi-

TABLE II. List of deep-inelastic virtual-photon-partonic subprocesses contributing to heavy-flavor production up to $O(\alpha_s^2)$. The one-loop corrections to the Born approximation have been included in our calculations, but are not explicitly mentioned in the table.

Order	Parton subprocess	Coefficient function
α_s^1	$\gamma^*+g\to Q+\bar{Q}$	$C_{k,g}^{H,(1)}$
α_s^2	$\gamma^*+g\to Q+\bar{Q}+g$	$C_{k,g}^{H,(2)}$
α_s^2	$\gamma^*+q(\bar{q})\to q(\bar{q})+Q+\bar{Q}$	$C_{k,q}^{H,(2)}$, $\mathcal{C}_{k,q}^{\mathrm{NS},(2)}=\mathcal{C}_{k,q}^{\mathrm{S},(2)}$

plication by a color factor

$$\mathcal{C}_{k,g}^{(1)}\left[z,\frac{Q^2}{M^2}\right]=n_f T_f \mathcal{C}_{k,\gamma}^{(0)}\left[z,\frac{Q^2}{M^2}\right] \quad (k=2,L) . \tag{2.35}$$

An analogous relation holds when the massless quarks in the final state are replaced by the heavy flavors (Table II) and we get, from (2.27) and (2.28),

$$\mathcal{C}_{k,g}^{H,(1)}(z,Q^2,m^2)=T_f \mathcal{C}_{k,\gamma}^{(0)}(z,Q^2,m^2) \quad (k=2,L) . \tag{2.36}$$

The color factors that appear in the above equations are given by $C_F=\frac{4}{3}$ and $T_f=\frac{1}{2}$ for the case of SU(3).

The higher-order α_s^2 corrections to the coefficient functions, describing massless partons only, are denoted by $\mathcal{C}_{k,i}^{(2)}$, where $i=q,g$ (see Table I). They have been calculated in [24]. In the Appendix we have decomposed $\mathcal{C}_{k,i}^{(2)}$ into color factors so that we can infer the $O(\alpha_s)$ photonic coefficients $\mathcal{C}_{k,\gamma}^{(1)}$ from the Abelian part of $\mathcal{C}_{k,g}^{(2)}$.

The $O(\alpha_s^2)$ corrections to the heavy-flavor coefficient functions given by $\mathcal{C}_{k,i}^{(2)}(z,Q^2/M^2,m^2)$ and $\mathcal{C}_{k,i}^{H,(2)}(z,Q^2/M^2,m^2)$ (Table II) are calculated for the first time in [25]. The relations between these coefficients and the ones derived in Sec. V of [25] will be presented in the Appendix. By decomposing them in color factors we again can derive the photonic heavy-flavor coefficient $\mathcal{C}_{k,\gamma}^{H,(1)}$ from the Abelian part of $\mathcal{C}_{k,g}^{H,(2)}$. Since in lowest order the hadronic heavy-flavor coefficient $\mathcal{C}_{k,i}^{(2)}(z,Q^2/M^2,m^2)$ only contributes up to the $O(\alpha_s^2)$ level, when $i=q$ we do not have to distinguish between singlet (S) and nonsinglet (NS) and we can put

$$\mathcal{C}_{k,q}^{\mathrm{S},(2)}\left[z,\frac{Q^2}{M^2},m^2\right]=\mathcal{C}_{k,q}^{\mathrm{NS},(2)}\left[z,\frac{Q^2}{M^2},m^2\right]=\mathcal{C}_{k,q}^{(2)}(z,Q^2,m^2) . \tag{2.37}$$

The above expression indicates that in lowest order $\mathcal{C}_{k,q}^{(2)}(z,Q^2,m^2)$ is determined without having performed mass factorization, which is indicated by its independence of the mass factorization scale M. This is because it originates from the Compton scattering process, which in lowest order does not have collinear singularities.

Finally, in Table III we have translated our notation for the coefficient functions into that used in [14,23,28,29]. We also list the new contributions to the photon structure functions which were not included earlier in the literature.

III. RESULTS

In this section we will discuss the NLO QCD corrections to the photon structure functions $F_k^\gamma(x,Q^2)$ for $(k=2,L)$. In particular, we focus our attention on the heavy-flavor contributions (mainly charm), which originate from the hadronic as well as the photonic coefficient functions in (2.6). Since heavy flavors can be produced either in virtual-photon parton or in virtual-photon real-photon reactions, we will call the former hadronic heavy-flavor production and the latter photonic heavy-flavor production.

In the subsequent part of this section we want to make a comparison between the LO and NLO description of the photon structure functions, where all contributions listed in Tables IV and V are included. Furthermore, we want to investigate the relative magnitude of the heavy-flavor (mainly charm) component of the structure function. We also show the difference between the massless and massive heavy-flavor approach. When the heavy quarks are treated as massless, their contribution to the photon structure functions are given by the correspond-

TABLE III. Notation in several papers for the hadronic and photonic coefficient functions. Notice that the expressions in [29] are in Mellin transform space. The blanks mean that these contributions were not considered in the papers quoted. The expressions with * can be found in [23], the ones with ** in [28].

This paper	[29]	[14]	[23]*, [28]**
$\mathcal{C}_{2,\gamma}^{(0)}$ (2.25)	$B_\gamma^{(n)}$ (4.12)	B_γ (3.7)	
$\frac{3\alpha_s}{4\pi}e_q^4\mathcal{C}_{L,\gamma}^{(0)}$ (2.26)			$\frac{1}{x}F_{L,q\bar{q}}^{\gamma,(0)}$ (15)*
$\frac{3\alpha_s}{4\pi}\left[\frac{2}{3}\right]^4\mathcal{C}_{2,\gamma}^{H,(0)}$ (2.27)			$\frac{1}{x}F_{2,c}^{\gamma}$ (2.13)**
$\frac{3\alpha_s}{4\pi}\left[\frac{2}{3}\right]^4\mathcal{C}_{L,\gamma}^{H,(0)}$ (2.28)			$\frac{1}{x}F_{L,q\bar{q}}^{\gamma,(0)}$ (16)*
$\mathcal{C}_{2,q}^{(1)}$ (2.33)	$B_{\mathrm{NS}}^{(n)},B_\psi^{(n)}$ (4.10)	B_{NS},B_q (3.7)	
$\mathcal{C}_{L,q}^{(1)}$ (2.34)			
$\mathcal{C}_{2,g}^{(1)}$ (2.35)	$B_{\mathrm{G}}^{(n)}$ (4.11)	B_{G} (3.7)	
$\mathcal{C}_{L,g}^{(1)}$ (2.35)			
$\mathcal{C}_{k,g}^{H,(1)}$ (2.36)			
$\mathcal{C}_{k,\gamma}^{(1)}$ [24]			
$\mathcal{C}_{k,\gamma}^{H,(1)}$ [25]			
$\mathcal{C}_{k,q}^{(2)}$ [24]			
$\mathcal{C}_{k,q}^{H,(2)}$ [25]			

TABLE IV. Coefficient functions used in this paper for a leading-order (LO) and a next-to-leading-order (NLO) analysis of $F_2^\gamma(x,Q^2)/\alpha$.

Order	Parton subprocess	Coefficient function
α_s^0	$\gamma^*+q(\bar{q})\to q(\bar{q})$	$\mathcal{C}_{2,q}^{(0)}$ LO
	$\gamma^*+\gamma\to q+\bar{q}$	$\mathcal{C}_{2,\gamma}^{(0)}$ NLO
	$\gamma^*+\gamma\to Q+\bar{Q}$	$\mathcal{C}_{2,\gamma}^{H,(0)}$ LO
α_s^1	$\gamma^*+q(\bar{q})\to q(\bar{q})+g$	$\mathcal{C}_{2,q}^{\mathrm{NS},(1)}$ $(=\mathcal{C}_{2,q}^{\mathrm{S},(1)})$ NLO
	$\gamma^*+g\to q+\bar{q}$	$\mathcal{C}_{2,g}^{(1)}$ NLO
	$\gamma^*+g\to Q+\bar{Q}$	$\mathcal{C}_{2,g}^{H,(1)}$ LO
	$\gamma^*+\gamma\to Q+\bar{Q}+g$	$\mathcal{C}_{2,\gamma}^{H,(1)}$ NLO
α_s^2	$\gamma^*+g\to Q+\bar{Q}+g$	$\mathcal{C}_{2,g}^{H,(1)}$ NLO
	$\gamma^*+q(\bar{q})\to q(\bar{q})+Q+\bar{Q}$	$\mathcal{C}_{2,q}^{H,(2)}$, $\mathcal{C}_{2,q}^{\mathrm{NS},(2)}$ $(=\mathcal{C}_{2,q}^{\mathrm{S},(2)})$ NLO

ing parton densities in the photon convoluted with the light-quark and gluon coefficient functions. This description is appropriate when $Q^2 \gg m^2$. If Q^2 is of the same order of magnitude as m^2, then the massive quark approach has to be adopted and the heavy-flavor production is described by the heavy-flavor coefficient functions in (2.6), which can be computed order by order in perturbation theory.

In the literature an LO analysis was given for $F_2^\gamma(x,Q^2)$ in [16] and $F_L^\gamma(x,Q^2)$ in [23]. Here all LO coefficient functions in Tables IV and V were included except for the ones related to hadronic heavy-flavor production (i.e., $\gamma^*+g\to Q+\bar{Q}$). The last contributions were also neglected in the NLO analysis for $F_2^\gamma(x,Q^2)$ in [19], and the photonic heavy-flavor contribution from $\gamma^*+\gamma\to Q+\bar{Q}$ was only taken into account in lowest order. An NLO analysis of $F_L^\gamma(x,Q^2)$ could not be carried out previously because the order α_s^2 contributions to all the longitudinal coefficient functions were not known until recently. Since all NLO coefficient functions are now known, and they are listed in Tables IV and V, we are able to present a complete NLO description for both $F_2^\gamma(x,Q^2)$ and for $F_L^\gamma(x,Q^2)$ so that one can make a comparison with the LO descriptions.

In our plots we adopt the LO and NLO parametrizations of the parton densities in the photon from [19] (for other sets, see [20,21]). For $n_f=3$ we use $\Lambda_{\mathrm{QCD}}=232$ MeV at leading order, and $\Lambda_{\mathrm{QCD}}=248$ MeV at next-to-leading order. For $n_f=4$, both the leading-order and the next-to-leading-order Λ_{QCD} are set equal to 200 MeV. In leading order, we adopt the one-loop result for the running coupling constant, and in next-to-leading order, we choose the two-loop corrected running coupling constant, as, e.g., given in Eq. (8) in [19]. All calculations are done by putting the factorization scale $M^2=Q^2$, unless indicated otherwise. In the case that the charm quark is treated as massive, its production is described by the heavy-flavor coefficient functions $\mathcal{C}_{k,i}^H$ $(k=2,L)$, and $(i=q,g,\gamma)$, and $\mathcal{C}_{k,q}$ in (2.6) (see also Tables IV and V) with $m_c=1.5$ GeV/c^2. Furthermore, the incoming light partons are given by u, d, s, and g, which are described by the parton densities given in [19]. In this case the number of light flavors is given by $n_f=3$, which has to be used in the running coupling constant as well as in the light parton coefficient functions.

If the charm is treated as massless, the incoming charm is described by a parton density in a similar way as is done for the light partons u, d, s, and g. The number of light flavors is now put to be $n_f=4$ and, in order to avoid double counting, the heavy-charm coefficient functions $\mathcal{C}_{k,i}^H$ $(k=2,L)$, $(i=q,g,\gamma)$, and $\mathcal{C}_{k,q}$ in (2.6) have to be omitted. Notice that the bottom- and top-quark contributions will be omitted, since they are negligible for the Q^2 values accessible at past and present experiments. In the subsequent part of the paper we will introduce the notation that $n_f=3$ stands for the massive charm approach,

TABLE V. Coefficient functions used in this paper for a leading order (LO) and a next-to-leading order (NLO) analysis of $F_L^\gamma(x,Q^2)/\alpha$.

Order	Parton subprocess	Coefficient function
α_s^0	$\gamma^*+\gamma\to q+\bar{q}$	$\mathcal{C}_{L,\gamma}^{(0)}$ LO
	$\gamma^*+\gamma\to Q+\bar{Q}$	$\mathcal{C}_{L,\gamma}^{H,(0)}$ LO
α_s^1	$\gamma^*+q(\bar{q})\to q(\bar{q})+g$	$\mathcal{C}_{L,q}^{\mathrm{NS},(1)}$ $(=\mathcal{C}_{L,q}^{\mathrm{S},(1)})$ LO
	$\gamma^*+g\to q+\bar{q}$	$\mathcal{C}_{L,g}^{(1)}$ LO
	$\gamma^*+g\to Q+\bar{Q}$	$\mathcal{C}_{L,g}^{H,(1)}$ LO
	$\gamma^*+\gamma\to q+\bar{q}+g$	$\mathcal{C}_{L,\gamma}^{(1)}$ NLO
	$\gamma^*+\gamma\to Q+\bar{Q}+g$	$\mathcal{C}_{L,\gamma}^{H,(1)}$ NLO
α_s^2	$\gamma^*+q(\bar{q})\to q(\bar{q})+g+g$	$\mathcal{C}_{L,q}^{\mathrm{NS},(2)}$ $(=\mathcal{C}_{L,q}^{\mathrm{S},(2)})$ NLO
	$\gamma^*+q(\bar{q})\to q(\bar{q})+q(\bar{q})+\bar{q}(q)$	$\mathcal{C}_{L,q}^{\mathrm{NS},(2)}$, $\mathcal{C}_{L,q}^{\mathrm{S},(2)}$ $(\neq\mathcal{C}_{L,q}^{\mathrm{NS},(2)})$ NLO
	$\gamma^*+g\to q+\bar{q}+g$	$\mathcal{C}_{L,g}^{(2)}$ NLO
	$\gamma^*+g\to Q+\bar{Q}+g$	$\mathcal{C}_{L,g}^{H,(2)}$ NLO
	$\gamma^*+q(\bar{q})\to q(\bar{q})+Q+\bar{Q}$	$\mathcal{C}_{L,q}^{H,(2)}$, $\mathcal{C}_{L,q}^{\mathrm{NS},(2)}$ $(=\mathcal{C}_{L,q}^{\mathrm{S},(2)})$ NLO

whereas $n_f=4$ indicates the massless charm description of the photon structure functions.

In the LO approximation the corresponding parton densities are multiplied by the coefficient functions in Tables IV and V, which are indicated by LO. In NLO we have chosen the $\overline{\text{MS}}$ scheme for the parton densities, the coefficient functions, and the running coupling constant. The coefficient functions which have to be added to the LO ones are indicated by NLO in Tables IV and V. In order to get a consistent NLO analysis for the structure functions we follow the procedure in [19], which is explained in [18]. Therefore we multiply the LO coefficient functions by f^γ, and the NLO coefficient functions by f_0^γ in (2.6) (for the notation of f^γ and f_0^γ, see Eq. (A23) and the discussion in Appendix A in [19]). Notice that in [19] the parton densities described in Appendix A were presented in the deep inelastic scattering for photons ($\overline{\text{DIS}}_\gamma$) scheme. However, they can be changed into the $\overline{\text{MS}}$ scheme via Eqs. (4)–(6) in [19]. After changing the lowest-order photonic coefficient function $C_{2,\gamma}^{(0)}$ in the DIS_γ scheme, we have checked that both schemes lead to the same result, provided the change of Eq. (4) in [18] is only applied to the parton density denoted by f^γ as defined above.

We now compare the results from our calculations for $F_2^\gamma(x,Q^2)$ first with data from PLUTO [1] [$Q^2=5.9$ $(\text{GeV}/c)^2$] and then with data from AMY [6] [$Q^2=51$ $(\text{GeV}/c)^2$]. We also show predictions for $F_L^\gamma(x,Q^2)$.

In Fig. 5 ($n_f=3$) we make a comparison between the LO and NLO approximation for $F_2^\gamma(x,Q^2)$ at $Q^2=5.9$ $(\text{GeV}/c)^2$, where the heavy-charm components (hadronic and photonic) are included. The low-x hump is due to charm production, which turns off at about $x=0.4$ (the threshold value). We also show separately the contributions due to massive charm production. When this contribution reaches its maximum value it constitutes about 20% of the structure function F_2^γ in LO, and 25% in NLO. The $O(\alpha_s)$ corrections to massive charm production are quite large, and amount to about 50% of the lowest-order charm component of F_2^γ. Furthermore, Fig. 5 reveals that the LO and NLO descriptions of F_2^γ are not very different. Note that the data also seem to indicate the presence of a charm component.

In Fig. 6 ($n_f=3$) we do the same for $F_L^\gamma(x,Q^2)$ at $Q^2=5.9$ $(\text{GeV}/c)^2$. This is for theoretical purposes only: there are no data presently available for F_L^γ at any value of Q^2. As in the case of F_2^γ, Fig. 6 shows that there is not much difference between the LO and NLO results for F_L^γ. However, the heavy-charm component of F_L^γ is less important than in the case of F_2^γ. At LO it is about 10% where this component reaches its maximum, whereas in NLO it amounts to about 25%. The latter is due to the fact that the $O(\alpha_s)$ corrections to the heavy-charm component of F_L^γ are as large as 100%.

In Fig. 7 ($n_f=3$) we present $F_2^\gamma(x,Q^2)$ at LO for three different choices of the mass factorization scale. Note that in this case the only variation is due to the parton densities. The variation in the M dependence is uniform over the whole x range. Notice that F_2^γ gets smaller as M decreases. In Fig. 8 ($n_f=3$) we do the same for $F_L^\gamma(x,Q^2)$ at $Q^2=5.9$ $(\text{GeV}/c)^2$. Here there is an additional scale dependence due to $\alpha_s(M^2)$, so that, contrary to F_2^γ, the longitudinal structure function F_L^γ gets larger as M decreases.

Figure 9 ($n_f=3$) shows again the scale dependence of F_2^γ, but now at NLO. There is now an additional scale dependence due to $\alpha_s(M^2)$ and the mass factorization scale logarithms of the type $\ln(Q^2/M^2)$ in the coefficient functions [see, e.g., (2.25) and (2.33)]. Note that the scale dependence is reduced over the whole x range compared to the LO case. For $x<0.4$ (above the charm threshold) there is almost no scale variation anymore. For $x>0.85$ we observe that, contrary to the LO approximation (Fig. 7), F_2^γ gets larger when M decreases.

In Fig. 10 ($n_f=3$) we show the same plots as in Fig. 9 for $F_L^\gamma(x,Q^2)$. The scale variation is small as in the LO

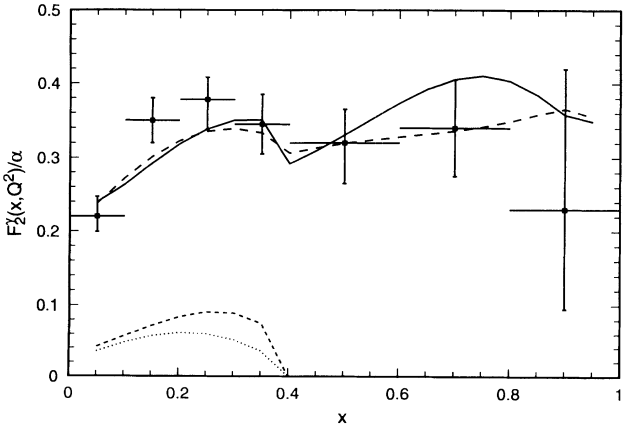

FIG. 5. The x dependence of $F_2^\gamma(x,Q^2)$ ($n_f=3$) at $Q^2=5.9$ $(\text{GeV}/c)^2$: solid line: F_2^γ(NLO); long-dashed line: F_2^γ(LO); short-dashed line: NLO heavy-charm contributions; dotted line: LO heavy-charm contributions. The data are from PLUTO [1].

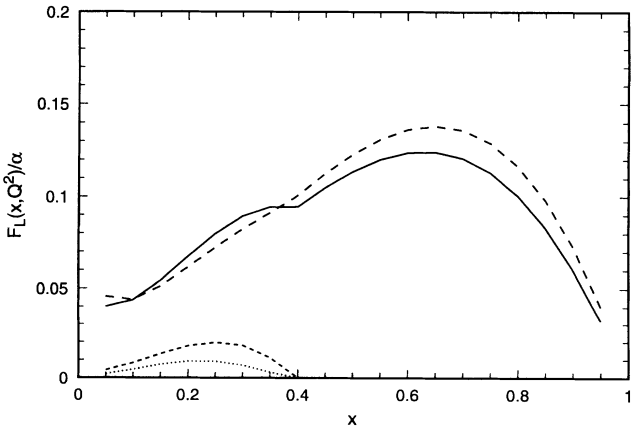

FIG. 6. The x dependence of $F_L^\gamma(x,Q^2)$ ($n_f=3$) at $Q^2=5.9$ $(\text{GeV}/c)^2$: solid line: F_L^γ(NLO); long-dashed line: F_L^γ(LO); short-dashed line: NLO heavy-charm contributions; dotted line: LO heavy-charm contributions.

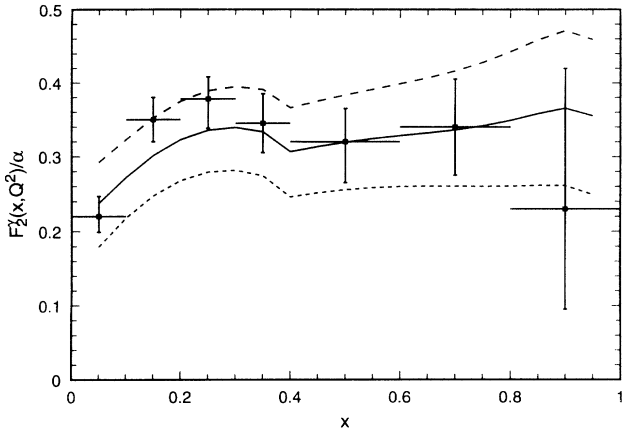

FIG. 7. The x dependence at LO of $F_2^\gamma(x,Q^2)$ ($n_f=3$) at $Q^2=5.9$ (GeV/c)^2 for three choices of the mass factorization scale M: $M=2Q$ (long-dashed line), $M=Q$ (solid line), and $M=Q/2$ (short-dashed line). The data are from PLUTO [1].

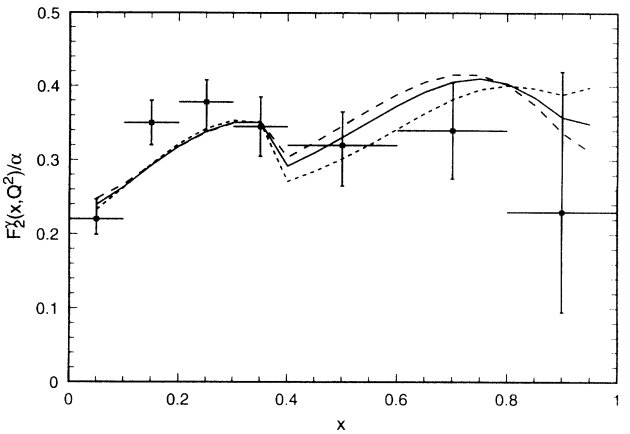

FIG. 9. The x dependence at NLO of $F_2^\gamma(x,Q^2)$ ($n_f=3$) at $Q^2=5.9$ (GeV/c)^2 for three choices of the mass factorization scale M: $M=2Q$ (long-dashed line), $M=Q$ (solid line), and $M=Q/2$ (short-dashed line). The data are from PLUTO [1].

case. Notice that in the NLO case there is a turning point at $x=0.4$ so that, when $x>0.4$, F_L^γ gets smaller for decreasing M.

We now turn to a comparison of results for the massive versus massless charm approach as discussed above. Since the differences are essentially the same in the LO case as in the NLO case, we only show plots for the latter. Therefore in Fig. 11 we compare the NLO ($n_f=3$) massive charm-quark approach to $F_2^\gamma(x,Q^2)$ at $Q^2=5.9$ (GeV/c)^2, with the NLO massless ($n_f=4$) description. For $x<0.4$ (above the charm threshold) the massless charm $n_f=4$ description leads to a result which is smaller than the one obtained from the massive charm approach ($n_f=3$). However, when $x>0.4$, where the charm contribution is zero, the massless charm approach provides us with larger values for F_2^γ than given by the massive charm description.

In Fig. 12 we show the same plots for $F_L^\gamma(x,Q^2)$ in NLO at $Q^2=5.9$ (GeV/c)^2. Note the enormous increase

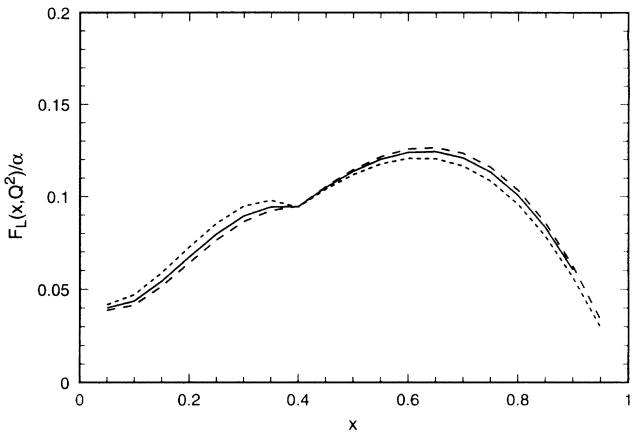

FIG. 10. The x dependence at NLO of $F_L^\gamma(x,Q^2)$ ($n_f=3$) at $Q^2=5.9$ (GeV/c)^2 for three choices of the mass factorization scale M: $M=2Q$ (long-dashed line), $M=Q$ (solid line), and $M=Q/2$ (short-dashed line).

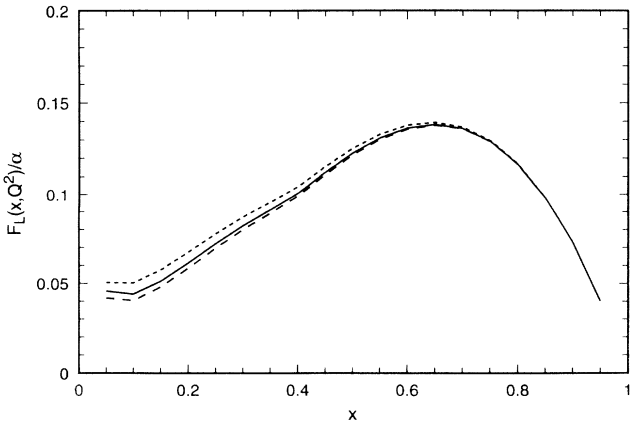

FIG. 8. The x dependence at LO of $F_L^\gamma(x,Q^2)$ ($n_f=3$) at $Q^2=5.9$ (GeV/c)^2 for three choices of the mass factorization scale M: $M=2Q$ (long-dashed line), $M=Q$ (solid line), and $M=Q/2$ (short-dashed line).

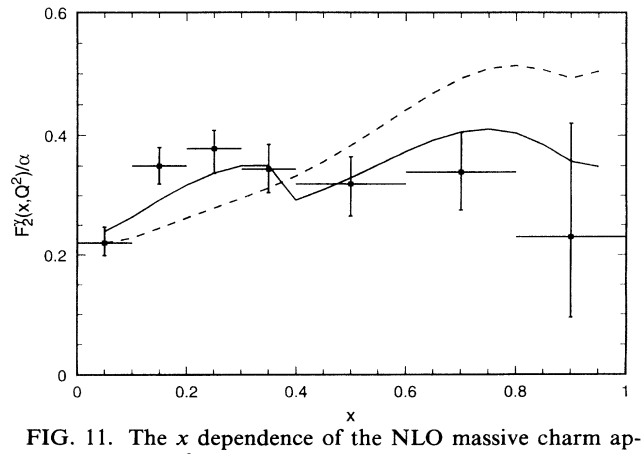

FIG. 11. The x dependence of the NLO massive charm approach to $F_2^\gamma(x,Q^2)$ ($n_f=3$, solid line) compared with the NLO massless charm description ($n_f=4$, dashed line), at $Q^2=5.9$ (GeV/c)^2. The data are from PLUTO [1].

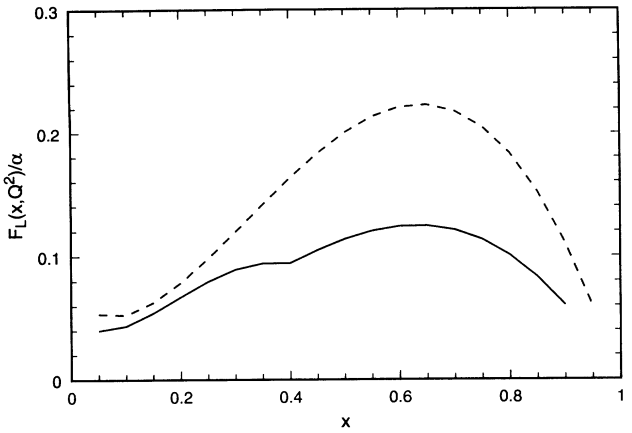

FIG. 12. The x dependence of the NLO massive charm approach to $F_L^\gamma(x,Q^2)$ ($n_f=3$, solid line) compared with the NLO massless charm description ($n_f=4$, dashed line), at $Q^2=5.9$ (GeV/c)^2.

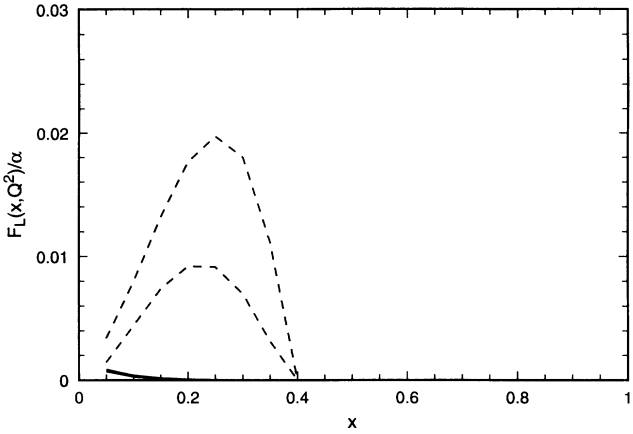

FIG. 14. The x dependence of the LO and NLO massive hadronic charm contributions to $F_L^\gamma(x,Q^2)$ ($n_f=3$) (solid lines) compared with the LO and NLO massive photonic charm contributions (dashed lines), at $Q^2=5.9$ (GeV/c)^2. The NLO contributions are the larger ones.

that occurs when we adopt the massless charm approach (dashed line). Since this effect is already there in the LO case, it can be understood as follows. In the case of $n_f=3$, where the charm is considered to be massive, one includes the light-quark coefficient function $\mathcal{C}_{L,\gamma}^{(0)}$ (2.26), which is multiplied by $\frac{2}{9}$, as well as the heavy-charm coefficient function $\mathcal{C}_{L,\gamma}^{H,(0)}$ (2.28), which is multiplied by $\frac{16}{81}$. When the charm is treated as massless with $n_f=4$, the coefficient function $\mathcal{C}_{L,\gamma}^{H,(0)}$ (massive charm) is replaced by $\mathcal{C}_{L,\gamma}^{(0)}$ (massless charm). For $x>0.4$ the former vanishes, but even for $x<0.4$ the massless charm coefficient function is much larger than the one for massive charm due to the threshold suppression factor in (2.28). This explains why the result for $n_f=4$ is much larger than for $n_f=3$. Notice that in the above arguments we have omitted the influence of the hadronic massive charm coefficient function $\mathcal{C}_{L,g}^{H,(1)}$ (2.36), which is negligible for $x>0.1$.

In Fig. 13 ($n_f=3$) we show the x dependences of the massive hadronic charm contribution and the massive photonic charm contribution to $F_2^\gamma(x,Q^2)$ at $Q^2=5.9$ (GeV/c)^2 in LO and in NLO. The corresponding results for $F_L^\gamma(x,Q^2)$ are shown in Fig. 14 ($n_f=3$) in LO and in NLO. The interesting feature to note in all these figures is that for $x>0.01$ the photonic charm component completely dominates the hadronic charm contribution. This makes $F_2^\gamma(x,Q^2)$ for massive charm production at moderate x a very promising test of PQCD because of the lack of dependence on the hadronic component. Experimentally, this is of course a very difficult quantity to determine, but perhaps not impossible. The same holds for $F_L^\gamma(x,Q^2)$ for massive charm production, but that is even more difficult to determine experimentally. However, for $x<0.01$ the pointlike contributions to both F_2^γ and F_L^γ for massive charm production become very small and the hadronic component begins to dominate.

We now repeat in Figs. 15–24 the previous Figs. 5–14

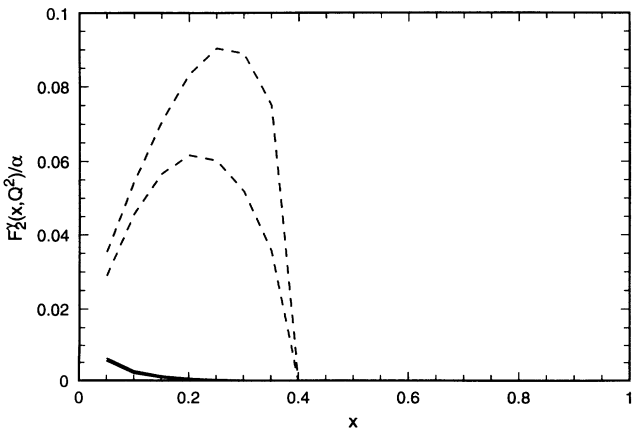

FIG. 13. The x dependence of the LO and NLO massive hadronic charm contributions to $F_2^\gamma(x,Q^2)$ ($n_f=3$) (solid lines) compared with the LO and NLO massive photonic charm contributions (dashed lines), at $Q^2=5.9$ (GeV/c)^2. The NLO contributions are the larger ones.

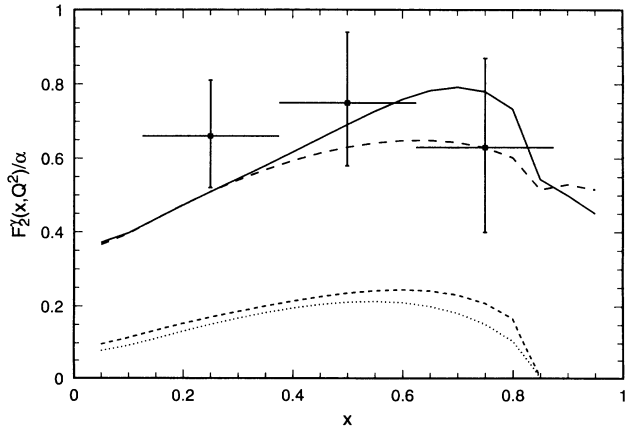

FIG. 15. The x dependence of $F_2^\gamma(x,Q^2)$ ($n_f=3$) at $Q^2=51$ (GeV/c)^2, solid line: F_2^γ(NLO); long-dashed line: F_2^γ(LO); short-dashed line: NLO heavy-charm contributions; dotted lines: LO heavy-charm contributions. The data are from AMY [6].

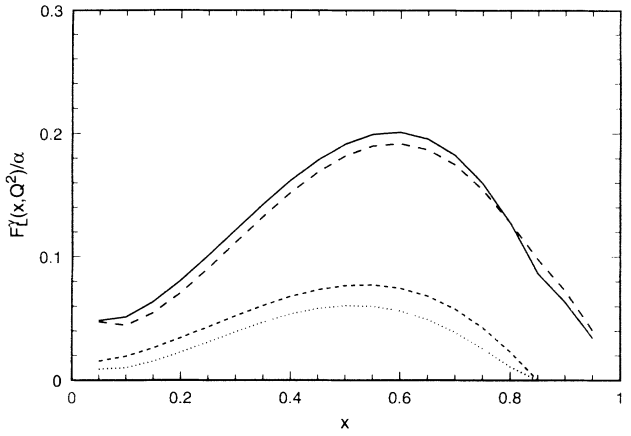

FIG. 16. The x dependence of $F_L^\gamma(x,Q^2)$ ($n_f=3$) at $Q^2=51$ (GeV/c)^2, solid line: F_L^γ(NLO), long dashed line: F_L^γ(LO), short dashed line: NLO heavy-charm contributions, dotted line: LO heavy-charm contributions.

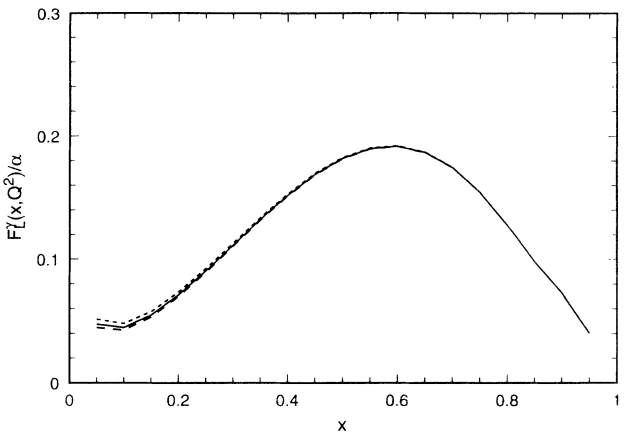

FIG. 18. The x dependence at LO of $F_L^\gamma(x,Q^2)$ ($n_f=3$) at $Q^2=51$ (GeV/c)^2 for three choices of the mass factorization scale M: $M=2Q$ (long-dashed line), $M=Q$ (solid line), and $M=Q/2$ (short-dashed line).

for the case $Q^2=51$ (GeV/c)^2 corresponding to the value for the AMY Collaboration. We remark that now the charm contribution switches off at $x=0.85$. Here the heavy-charm component becomes, in general, larger than in the case for $Q^2=5.9$ (GeV/c)^2. For F_2^γ it is 30% in LO and NLO, where this component reaches its maximum. For F_L^γ the percentages are 30 and 40, respectively. The $O(\alpha_s)$ corrections to heavy-charm production are smaller than for $Q^2=5.9$ (GeV/c)^2. For F_2^γ they are up to 20% and for F_L^γ up to 30% of the lowest-order charm component. The mass factorization scale dependence for $F_k^\gamma(x,Q^2)$ ($k=2,L$) is appreciably reduced compared to the case of $Q^2=5.9$ (GeV/c)^2. This holds for LO (Figs. 17 and 18) as well as NLO (Figs. 19 and 20). It can mainly be attributed to a smaller value of α_s because Q^2 is now larger.

In Figs. 21 (F_2^γ) and Fig. 22 (F_L^γ) we make the same comparison between the massive ($n_f=3$) and massless ($n_f=4$) charm approach as is done in Figs. 11 and 12, but now at $Q^2=51$ (GeV/c)^2. A comparison between Figs. 11 and 12 on the one hand and Figs. 21 and 22 on the other hand reveals that the difference between these two approaches becomes larger for F_2^γ as Q^2 increases, whereas for F_L^γ we observe the opposite. For F_L^γ this is easy to understand because $\mathcal{C}_{L,\gamma}^{H,(0)}$ (2.28) turns into $\mathcal{C}_{L,\gamma}^{(0)}$ (2.26) when $Q^2\to\infty$ and the threshold suppression factor in the former disappears. However, in the case of F_2^γ the physics is completely different. Here $\mathcal{C}_{2,\gamma}^{H,(0)}$ (2.27) [the same also holds for $\mathcal{C}_{2,g}^{H,(1)}$ (2.36)] diverges like

$$\mathcal{C}_{2,\gamma}^{H,(0)}(z,Q^2,m^2) \underset{Q^2\to\infty}{\sim} \mathcal{C}_{2,\gamma}^{(0)}(z,Q^2)+P_{c\gamma}^{(0)}(z)\ln\frac{M^2}{m^2}\ , \qquad (3.1)$$

where $P_{c\gamma}^{(0)}(z)$ is the Altarelli-Parisi (AP) splitting func-

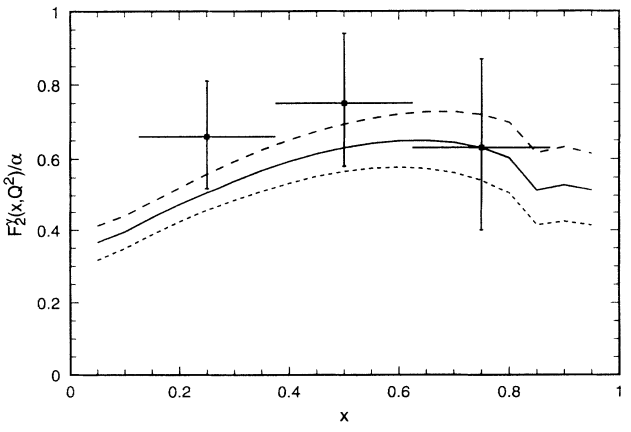

FIG. 17. The x dependence at LO of $F_2^\gamma(x,Q^2)$ ($n_f=3$) at $Q^2=51$ (GeV/c)^2 for three choices of the mass factorization scale M: $M=2Q$ (long dashed line), $M=Q$ (solid line), and $M=Q/2$ (short dashed line). The data are from AMY [6].

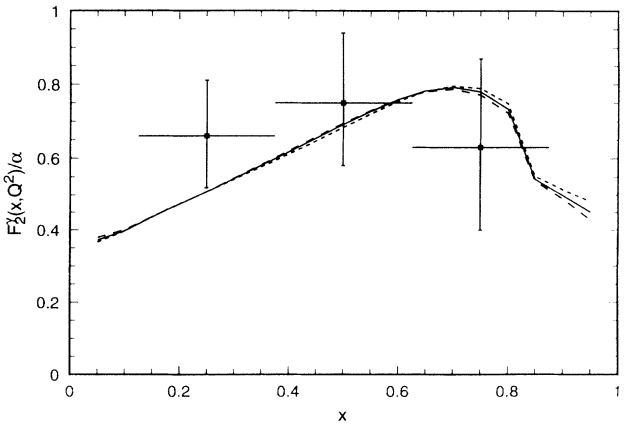

FIG. 19. The x dependence at NLO of $F_2^\gamma(x,Q^2)$ ($n_f=3$) at $Q^2=51$ (GeV/c)^2 for three choices of the mass factorization scale M: $M=2Q$ (long-dashed line), $M=Q$ (solid line), and $M=Q/2$ (short-dashed line). The data are from AMY [6].

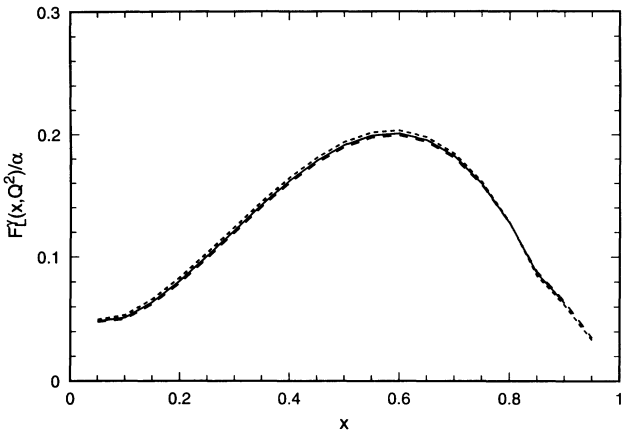

FIG. 20. The x dependence at NLO of $F_L^\gamma(x,Q^2)$ ($n_f=3$) at $Q^2=51$ (GeV/c)^2 for three choices of the mass factorization scale M: $M=2Q$ (long-dashed line), $M=Q$ (solid line), and $M=Q/2$ (short-dashed line).

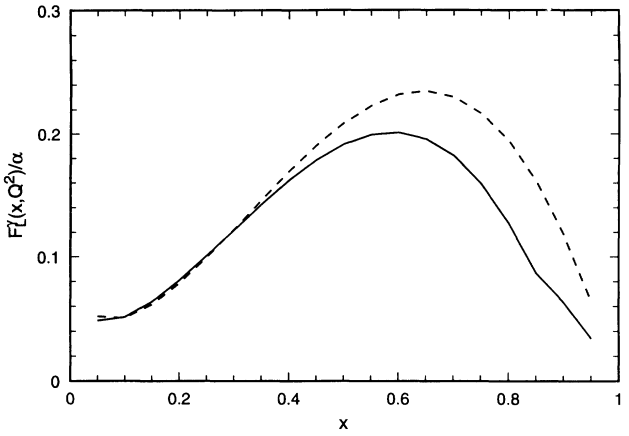

FIG. 22. The x dependence of the NLO massive charm approach to $F_L^\gamma(x,Q^2)$ ($n_f=3$, solid line) compared with the NLO massless charm description ($n_f=4$, dashed line), at $Q^2=51$ (GeV/c)^2.

tion occurring in the splitting $\gamma\to c\bar{c}$ and $\mathcal{C}_{2,\gamma}^{(0)}$ is given in (2.25). The logarithmic term $\ln(M^2/m^2)$ has to be resummed according to the AP equations, and $\mathcal{C}_{2,\gamma}^{(0)}$ appears in the next-to-leading order to the same equations. In this way one absorbs expression (3.1) in the charm-parton density, and this defines the massless charm approach. Notice that this also happens for the higher-order coefficient functions $\mathcal{C}_{L,\gamma}^{H,(1)}$ contributing to F_L^γ, but this effect is suppressed by α_s. Above the charm threshold the massless charm approach ($n_f=4$) gives an equally good description as the massive charm approximation ($n_f=3$), since the lowest-order Bethe-Heitler process, represented by $\mathcal{C}_{2,\gamma}^{H,(0)}$, is somehow buried in the parton densities. However, close to threshold and below [$x>0.8$ for $Q^2=51$ (GeV/c)^2], both approaches start to deviate from each other. This is no surprise because in the case of $n_f=3$ the charm component in this region is suppressed, whereas it is still present for $n_f=4$ even at large x values. We believe that for moderate Q^2 values [$5<Q^2<100$ (GeV/c)^2] and $x>0.1$ the massive charm approach ($n_f=3$) is better, since we are relatively close to threshold: $W^2=Q^2(1-x)/x\geq 4m_c^2$ (see also the remark in the fourth line, right column on page 1974 of Ref. [19]).

To conclude, we have presented in this paper the first complete NLO analysis of $F_2^\gamma(x,Q^2)$ and $F_L^\gamma(x,Q^2)$ containing both light and heavy quarks. Summarizing our findings, we have seen that for both values of Q^2 the NLO structure functions are not too different from the LO ones. This is not so surprising for $F_2^\gamma(x,Q^2)$, since we used the parton densities of [19] and most of the contributions were already included in their NLO analysis except for the $O(\alpha_s)$ corrections to heavy-quark production and the contributions due to hadronic charm production, which are numerically small. We see that the mass fac-

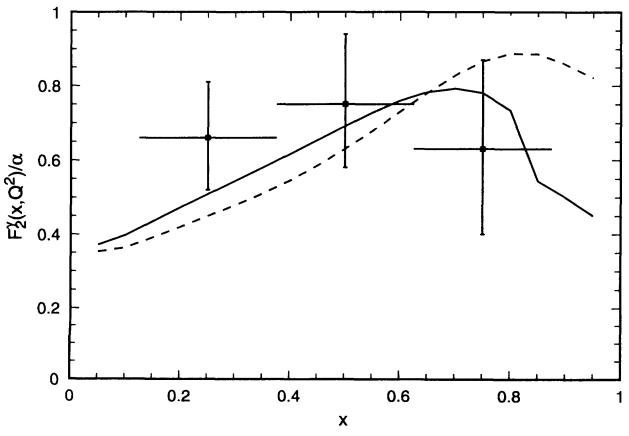

FIG. 21. The x dependence of the NLO massive charm approach to $F_2^\gamma(x,Q^2)$ ($n_f=3$, solid line) compared with the NLO massless charm description ($n_f=4$, dashed line), at $Q^2=51$ (GeV/c)^2. The data are from AMY [6].

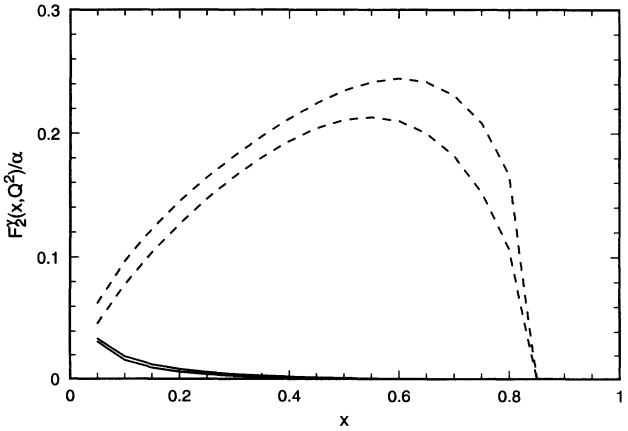

FIG. 23. The x dependence of the LO and NLO massive hadronic charm contributions to $F_2^\gamma(x,Q^2)$ ($n_f=3$) (solid lines) compared with the LO and NLO massive photonic charm contributions (dashed lines), at $Q^2=51$ (GeV/c)^2. The NLO contributions are the larger ones.

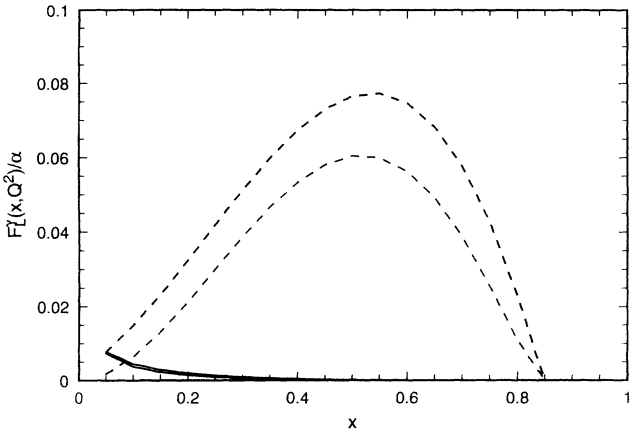

FIG. 24. The x dependence of the LO and NLO massive hadronic charm contributions to $F_L^\gamma(x,Q^2)$ ($n_f=3$) (solid line) compared with the LO and NLO massive photonic charm contributions (dashed lines), at $Q^2=51$ (GeV/c)^2. The NLO contributions are the larger ones.

torization scale independence of F_2^γ is considerably improved while going from the LO to the NLO approximation.

For $F_L^\gamma(x,Q^2)$ this is the first NLO analysis, and at the same time complete, since all heavy- and light-quark contributions have been included. We find that $F_L^\gamma(x,Q^2)$ changes very little from LO to NLO and is very stable under scale changes. Above $x\approx 0.1$ the hadronic production of charm is small compared with the photonic production, while the former is dominant for $x<0.01$. All this would make a measurement of $F_L^\gamma(x,Q^2)$ (e.g., at LEP 2) an interesting prospect.

Our results could be used to determine more accurate NLL parton distribution functions for the photon. This would become especially relevant when data become available for F_2^γ for charm production, and for F_L^γ. Finally, we stress that, if the heavy-quark contribution could be extracted from a measurement of F_2^γ, this would yield a very good test of perturbative QCD.

ACKNOWLEDGMENTS

The work in this paper was supported in part under Contract Nos. NSF 92-11367 and DOE DE-AC02-76CH03000. Financial support was also provided by the Texas National Research Laboratory Commission. S.R. would like to thank Fermilab for their hospitality while this paper was being completed. Furthermore, we would like to thank A. Vogt for his help in using the parton density program of [19].

APPENDIX

In this appendix we show how one can derive the $O(\alpha_s^2)$ coefficients corresponding to the reactions in Tables I and II from the expressions calculated in [24] and [25], respectively. The $O(\alpha_s^2)$ coefficients mentioned in Table I are given by

$$\mathcal{C}_{k,q}^{\mathrm{NS},(2)}\left[z,\frac{Q^2}{M^2}\right]=C_F^2 B_{FF}^{(k)}\left[z,\frac{Q^2}{M^2}\right]+C_A C_F B_{AF}^{(k)}\left[z,\frac{Q^2}{M^2}\right]+n_f T_F C_F B_{FF}^{(k)}\left[z,\frac{Q^2}{M^2}\right], \tag{A1}$$

where $\mathcal{C}_{L,q}^{\mathrm{NS},(2)}$ and $\mathcal{C}_{2,q}^{\mathrm{NS},(2)}$ are the coefficients of the $(\alpha_s/4\pi)^2$ term in Eqs. (B1) and (B2) of [24], respectively. The singlet coefficients can be split into a nonsinglet and a pure singlet piece as follows:

$$\mathcal{C}_{k,q}^{\mathrm{S},(2)}\left[z,\frac{Q^2}{M^2}\right]=\mathcal{C}_{k,q}^{\mathrm{NS},(2)}\left[z,\frac{Q^2}{M^2}\right]+\mathcal{C}_{k,q}^{\mathrm{PS},(2)}\left[z,\frac{Q^2}{M^2}\right]. \tag{A2}$$

The pure singlet coefficients $\mathcal{C}_{k,q}^{\mathrm{PS},(2)}$ can be written as

$$\mathcal{C}_{k,q}^{\mathrm{PS},(2)}\left[z,\frac{Q^2}{M^2}\right]=n_f T_f C_F D_{FF}^{(k)}\left[z,\frac{Q^2}{M^2}\right], \tag{A3}$$

where $\mathcal{C}_{L,q}^{\mathrm{PS},(2)}$ and $\mathcal{C}_{2,q}^{\mathrm{PS},(2)}$ are the coefficients of the $(\alpha_s/4\pi)^2$ terms in Eqs. (B3) and (B4) of [24], respectively. Finally, the gluonic coefficient is given by

$$\mathcal{C}_{k,g}^{(2)}\left[z,\frac{Q^2}{M^2}\right]=n_f T_f C_F E_{FF}^{(k)}\left[z,\frac{Q^2}{M^2}\right]+n_f T_f C_A E_{FA}^{(k)}\left[z,\frac{Q^2}{M^2}\right], \tag{A4}$$

where $\mathcal{C}_{L,g}^{(2)}$ and $\mathcal{C}_{2,g}^{(2)}$ are the coefficients of the $(\alpha_s/4\pi)^2$ terms in Eqs. (B5) and (B6) of [24], respectively. The color factors in SU(3) are given by $C_F=4/3$, $C_A=3$, and $T_F=1/2$, and n_f denotes the number of light flavors. The $O(\alpha_s)$ photonic coefficient $\mathcal{C}_{k,\gamma}^{(1)}$ can be derived from the Abelian part of $\mathcal{C}_{k,g}^{(2)}$ (A4) and it equals

$$\mathcal{C}_{k,\gamma}^{(1)}\left[z,\frac{Q^2}{M^2}\right]=C_F E_{FF}^{(k)}\left[z,\frac{Q^2}{M^2}\right]. \tag{A5}$$

The coefficient functions due to heavy flavor production (see Table II) are related to the coefficients defined in [25] in the following way. In first order in α_s we have [see also (2.36)]

$$\mathcal{C}_{L,g}^{H,(1)}(z,Q^2,m^2)=\frac{1}{\pi}\frac{Q^2}{m^2 z}c_{L,g}^{(0)}(\eta,\xi), \tag{A6}$$

$$\mathcal{C}_{2,g}^{H,(1)}(z,Q^2,m^2)=\frac{1}{\pi}\frac{Q^2}{m^2 z}[c_{T,g}^{(0)}(\eta,\xi)+c_{L,g}^{(0)}(\eta,\xi)], \tag{A7}$$

with

$$\eta=\frac{s}{4m^2}-1,\quad \xi=\frac{Q^2}{m^2}. \tag{A8}$$

In second order in α_s one gets, for $i=q,g$,

$$\mathcal{C}_{L,q}^{(2)}(z,Q^2,m^2)=16\pi\frac{Q^2}{m^2 z}d_{L,q}^{(1)}(\eta,\xi), \tag{A9}$$

$$\mathcal{C}_{2,g}^{(2)}(z,Q^2,m^2)=16\pi\frac{Q^2}{m^2 z}[d_{T,q}^{(1)}(\eta,\xi)+d_{L,q}^{(1)}(\eta,\xi)] , \tag{A10}$$

and

$$\mathcal{C}_{L,i}^{H,(2)}\left[z,\frac{Q^2}{M^2},m^2\right] =16\pi\frac{Q^2}{m^2 z}\left[c_{L,i}^{(1)}(\eta,\xi)+\bar{c}_{L,i}^{(1)}(\eta,\xi)\ln\frac{M^2}{m^2}\right] , \tag{A11}$$

$$\mathcal{C}_{2,i}^{H,(2)}\left[z,\frac{Q^2}{M^2},m^2\right]=16\pi\frac{Q^2}{m^2 z}\left[c_{T,i}^{(1)}(\eta,\xi)+c_{L,i}^{(1)}(\eta,\xi) +[\bar{c}_{T,i}^{(1)}(\eta,\xi)+\bar{c}_{L,i}^{(1)}(\eta,\xi)] \times\ln\frac{M^2}{m^2}\right] . \tag{A12}$$

In the above expressions the coefficients $c_{k,i}^{(1)},\bar{c}_{k,i}^{(1)}$, and $d_{k,i}^{(1)}$ for $(k=T,L)$ and $(i=q,g)$ are defined in Eqs. (5.3)–(5.6) of [25]. As has already been mentioned, they are too long to be presented in a paper and they are available upon request. Like the coefficient functions in Table I, the heavy-flavor contributions can be decomposed in color factors in a similar way. In first order in α_s we have

$$\mathcal{C}_{k,g}^{H,(1)}(z,Q^2,m^2)=T_f\mathcal{C}_{k,\gamma}^{H,(0)}(z,Q^2,m^2) , \tag{A13}$$

where $\mathcal{C}_{k,\gamma}^{H,(0)}$ denotes the photonic coefficient which is given in Eqs. (2.27) and (2.28) [see also (2.36)]. In second order in α_s the expressions are analogous to the ones presented for light-quark production in (A1), (A3), and (A4):

$$\mathcal{C}_{k,q}^{(2)}(z,Q^2,m^2)=T_f C_F B_{FF}^{(k)}(z,Q^2,m^2) , \tag{A14}$$

$$\mathcal{C}_{k,q}^{H,(2)}\left[z,\frac{Q^2}{M^2},m^2\right]=T_f C_F D_{FF}^{(k)}\left[z,\frac{Q^2}{M^2},m^2\right] , \tag{A15}$$

and

$$\mathcal{C}_{k,g}^{H,(2)}\left[z,\frac{Q^2}{M^2},m^2\right]=T_f C_F E_{FF}^{(k)}\left[z,\frac{Q^2}{M^2},m^2\right] +T_f C_A E_{FA}^{(k)}\left[z,\frac{Q^2}{M^2},m^2\right] . \tag{A16}$$

Notice that in the limit $m\to 0$ the above expressions need an additional mass factorization. After this procedure is carried out, the coefficients B_{FF}, D_{FF}, E_{FF}, and E_{FA} pass into their massless analogues defined in (A1), (A3), and (A4). The order α_s contributions to the photonic coefficient function $\mathcal{C}_{k,\gamma}^{H}$ can be derived from (A16). It is equal to

$$\mathcal{C}_{k,\gamma}^{H,(1)}(z,Q^2,m^2)=C_F E_{FF}^{(k)}(z,Q^2,m^2) . \tag{A17}$$

[1] PLUTO Collaboration, Ch. Berger *et al.*, Phys. Lett **107B**, 168 (1981); **142B**, 111 (1984); **149B**, 421 (1984); Z. Phys. C **26**, 353 (1984); Nucl. Phys. **B281**, 365 (1987).

[2] CELLO Collaboration, H. J. Behrend *et al.*, Phys. Lett. **126B**, 391 (1983); C. Kiesling, in *Proceedings of the XXV International Conference on High Energy Physics,* Singapore, 1990, edited by K. K. Phua and Y. Yamaguchi (World Scientific, Singapore, 1990).

[3] TPC2γ Collaboration, H. Aihara *et al.*, Phys. Rev. Lett. **58**, 97 (1987); Z. Phys. C **34**, 1 (1987); D. Bintinger *et al.*, Phys. Rev. Lett. **54**, 763 (1985).

[4] TASSO Collaboration, M. Althoff *et al.*, Z. Phys. C **31**, 527 (1986).

[5] JADE Collaboration, W. Bartel *et al.*, Z. Phys. C **24**, 231 (1984); Phys. Lett. **121B**, 205 (1983).

[6] AMY Collaboration, R. Tanaka, in *Photon-Photon '92, Proceedings of the IX International Workshop on Photon-Photon Collisions,* San Diego, California, 1992, edited by D. O. Caldwell and H. P. Paar (World Scientific, Singapore, 1992); R. Tanaka *et al.*, Phys. Lett. B **277**, 215 (1992); T. Sasaki *et al.*, *ibid.* **252**, 491 (1990); T. Nozaki, in *Proceedings of the Joint International Lepton-Photon Symposium and Europhysics Conference on High Energy Physics,* Geneva, Switzerland, 1991, edited by S. Hegarty, K. Potter, and E. Quercigh (World Scientific, Singapore, 1991), p. 156.

[7] VENUS Collaboration, M. Chiba, in *High Energy Hadronic Interactions,* Proceedings of the XXVIth Rencontres de Moriond, Les Arcs, France, 1991, edited by J. Tran Thanh Van (Editions Frontieres, Gif-sur-Yvette, 1991).

[8] TOPAZ Collaboration, H. Hayashii, in *Photon-Photon '92* [6].

[9] A. Ali *et al.*, in *Physics at LEP,* LEP Jamboree, Geneva, Switzerland, 1985, edited by J. Ellis and R. Peccei (CERN Report No. 86-02, Geneva, 1986), Vol. 2, p. 81.

[10] M. Drees and R. M. Godbole, DESY Report No. 92-044; Phys. Rev. Lett. **67**, 1189 (1991).

[11] O. J. P. Éboli, M. C. Gonzalez-Garcia, F. Halzen, and S. F. Novaes, Phys. Rev. D **47**, 1889 (1993); M. Drees, M. Krämer, J. Zunft, and P. M. Zerwas, Phys. Lett. B **306**, 371 (1993); J. H. Kühn, E. Mirkes, and J. Steegborn, Z. Phys. C **57**, 615 (1993).

[12] E. Witten, Nucl. Phys. **B120**, 189 (1977).

[13] W. A. Bardeen, in *Proceedings of the 1981 International Symposium on Lepton and Photon Interactions at High Energies,* Bonn, Germany, edited by W. Pfeil (Physikalisches Institut, Universität Bonn, Bonn, 1981), p. 432.

[14] M. Glück and E. Reya, Phys. Rev. D **28**, 2749 (1983).

[15] J. H. Field, in *Photon-Photon Collisions, Proceedings of the VIII International Workshop on Photon-Photon Collisions,* Shoresh, Israel, 1988, edited by U. Karshon (World Scientific, Singapore, 1989), p. 349; S. Kawabata, in *Proceedings of the Joint International Lepton-Photon Symposium and Europhysics Conference on High Energy Physics* [6], p. 53.

[16] M. Drees and K. Grassie, Z. Phys. C **28**, 451 (1985).

[17] H. Abramowicz, K. Charchula, and A. Levy, Phys. Lett. B **269**, 458 (1991); see also H. Abramowicz *et al.*, DESY Report No. 91-057 (unpublished).

[18] M. Glück, E. Reya, and A. Vogt, Phys. Rev. D **45**, 3986

(1992).
[19] M. Glück, E. Reya, and A. Vogt, Phys. Rev. D **46**, 1973 (1992).
[20] P. Aurenche, P. Chiapetta, M. Fontannaz, J. Ph. Guillet, and E. Pilon, Nucl. Phys. **B399**, 34 (1993).
[21] L. E. Gordon and J. K. Storrow, Z. Phys. C **56**, 307 (1992).
[22] J. H. Field, F. Kapusta, and L. Poggioli, Z. Phys. C **36**, 121 (1987); Phys. Lett. B **181**, 362 (1986); J. H. Da Luz Vieira and J. K. Storrow, Z. Phys. C **51**, 241 (1991).
[23] M. Drees, M. Glück, and E. Reya, Phys. Rev. D **30**, 2316 (1984).
[24] E. B. Zijlstra and W. L. van Neerven, Nucl. Phys. **B383**, 525 (1992); Phys. Lett. B **273**, 476 (1991); W. L. van Neerven and E. B. Zijlstra, *ibid.* **272**, 127 (1991).
[25] E. Laenen, S. Riemersma, J. Smith, and W. L. van Neerven, Nucl. Phys. **B392**, 162 (1993); **B392**, 229 (1993); Phys. Lett. B **291**, 325 (1992).
[26] C. T. Hill and G. G. Ross, Nucl. Phys. **B148**, 373 (1979).
[27] J. Smith and W. L. van Neerven, Nucl. Phys. **B374**, 36 (1992).
[28] M. Glück, K. Grassie, and E. Reya, Phys. Rev. D **30**, 1447 (1984).
[29] W. A. Bardeen and A. J. Buras, Phys. Rev. D **20**, 166 (1979); **21**, 2041(E) (1980).
[30] M. Fontannaz and E. Pilon, Phys. Rev. D **45**, 382 (1992).
[31] E. Witten, Nucl. Phys. **B104**, 445 (1976); J. Babcock and D. Sivers, Phys. Rev. D **18**, 2301 (1978); M. A. Shifman, A. I. Vainstein, and V. J. Zakharov, Nucl. Phys. **B136**, 157 (1978); M. Glück and E. Reya, Phys. Lett. **83B**, 98 (1979); J. V. Leveille and T. Weiler, Nucl. Phys. **B147**, 147 (1979).
[32] M. Glück, in *Proceedings of the HERA Workshop,* Hamburg, Germany, 1987, edited by R. D. Peccei (DESY, Hamburg, 1988), Vol. 1, p. 119; M. Glück, R. M. Godbole, and E. Reya, Z. Phys. C **38**, 441 (1988).